

Investigation of unconventional reconstruction and electronic properties on the Na_2IrO_3 surface

F. Lüpke,^{1,2} S. Manni,^{3,4} S. C. Erwin,⁵ I. I. Mazin,⁵ P. Gegenwart,⁴ and M. Wenderoth^{1,*}

¹*IV. Physikalisches Institut, Georg-August-Universität Göttingen, D-37077 Göttingen, Germany*

²*Peter Grünberg Institut (PGI-3), Forschungszentrum Jülich, 52425 Jülich, Germany*

³*I. Physikalisches Institut, Georg-August-Universität Göttingen, D-37077 Göttingen, Germany*

⁴*Experimental Physics VI, Center for Electronic Correlations and Magnetism,*

University of Augsburg, D-86159 Augsburg, Germany

⁵*Center for Computational Materials Science, Naval Research Laboratory, Washington, DC 20375, USA*

(Dated: November 7, 2021)

Na_2IrO_3 is an intriguing material for which spin-orbit coupling plays a key role. Theoretical predictions, so far unverified, have been made that the surface of Na_2IrO_3 should exhibit a clear signature of the quantum spin Hall effect. We studied the surface of Na_2IrO_3 using scanning tunneling microscopy and density-functional theory calculations. We observed atomic level resolution of the surface and two types of terminations with different surface periodicity and Na content. By comparing bias-dependent experimental topographic images to simulated images, we determined the detailed atomistic structure of both observed surfaces. One of these reveals a strong relaxation to the surface of Na atoms from the subsurface region two atomic layers below. Such dramatic structural changes at the surface cast doubt on any prediction of surface properties based on bulk electronic structure. Indeed, using spatially resolved tunneling spectroscopy we found no indication of the predicted quantum spin Hall behavior.

PACS numbers: 75.40.Cx, 75.10.Jm, 75.40.Gb, 75.50.Lk

Novel states with unusual topological and frustrated properties have recently been predicted to arise in heavy transition-metal oxides, such as iridates, from a combination of interactions—spin-orbit coupling, Coulomb correlations, Hund’s rule coupling, and one-electron hopping—with comparable energy scales [1–7]. Na_2IrO_3 is a prototypical material in the iridate family. It consists of an alternating stacking of honeycomb Ir_2NaO_6 layers separated by hexagonal Na_3 layers [8]. While many works have concentrated on unusual magnetic properties of the bulk material, the surface of Na_2IrO_3 may also reveal unusual physics. For example, recent theoretical work predicts quantum spin Hall (QSH) behavior in Na_2IrO_3 [2]. The resulting band topology of the bulk should lead to helical edge states at the surface, which would be manifested experimentally by the closing of the band gap [2].

The prediction of QSH behavior was based on a tight-binding model derived from the bulk electronic structure [2]. It was subsequently shown that the bulk states depend very sensitively on the assumed geometry—in particular, on the positions of Na and corresponding rotations of the IrO_6 octahedra [7]. An important question, so far unaddressed, is whether the geometry at the surface of Na_2IrO_3 is sufficiently similar to the bulk to support the assumptions underlying the QSH prediction. In this Letter, we used scanning tunneling microscopy (STM) and spectroscopy (STS) together with density-functional theory (DFT) calculations to address this question. We also tested the QSH prediction directly by spectroscopically probing for gap closure on the surface. Our most important findings are that (1) the surface of Na_2IrO_3 strongly reconstructs in a highly un-

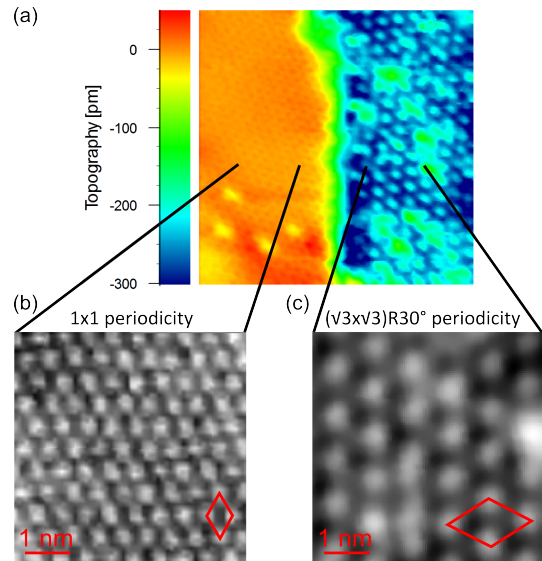


FIG. 1. (Color online) Constant-current STM topographic images at $V_{\text{bias}} = +2$ V. (a) Two different surface configurations with well-defined boundaries are observed. (b) Detail of the 1×1 surface and (c) $(\sqrt{3} \times \sqrt{3})R30^\circ$ surface, with the respective unit cells indicated. The 1×1 surface exhibits long-range order, while the $(\sqrt{3} \times \sqrt{3})R30^\circ$ surface exhibits many defects and only local order.

conventional manner, which very likely undermines the conditions for QSH behavior; (2) the surface band gap does *not* close, which establishes that QSH behavior is indeed not realized at the Na_2IrO_3 surface.

Na_2IrO_3 surfaces were prepared by in situ cleaving at a

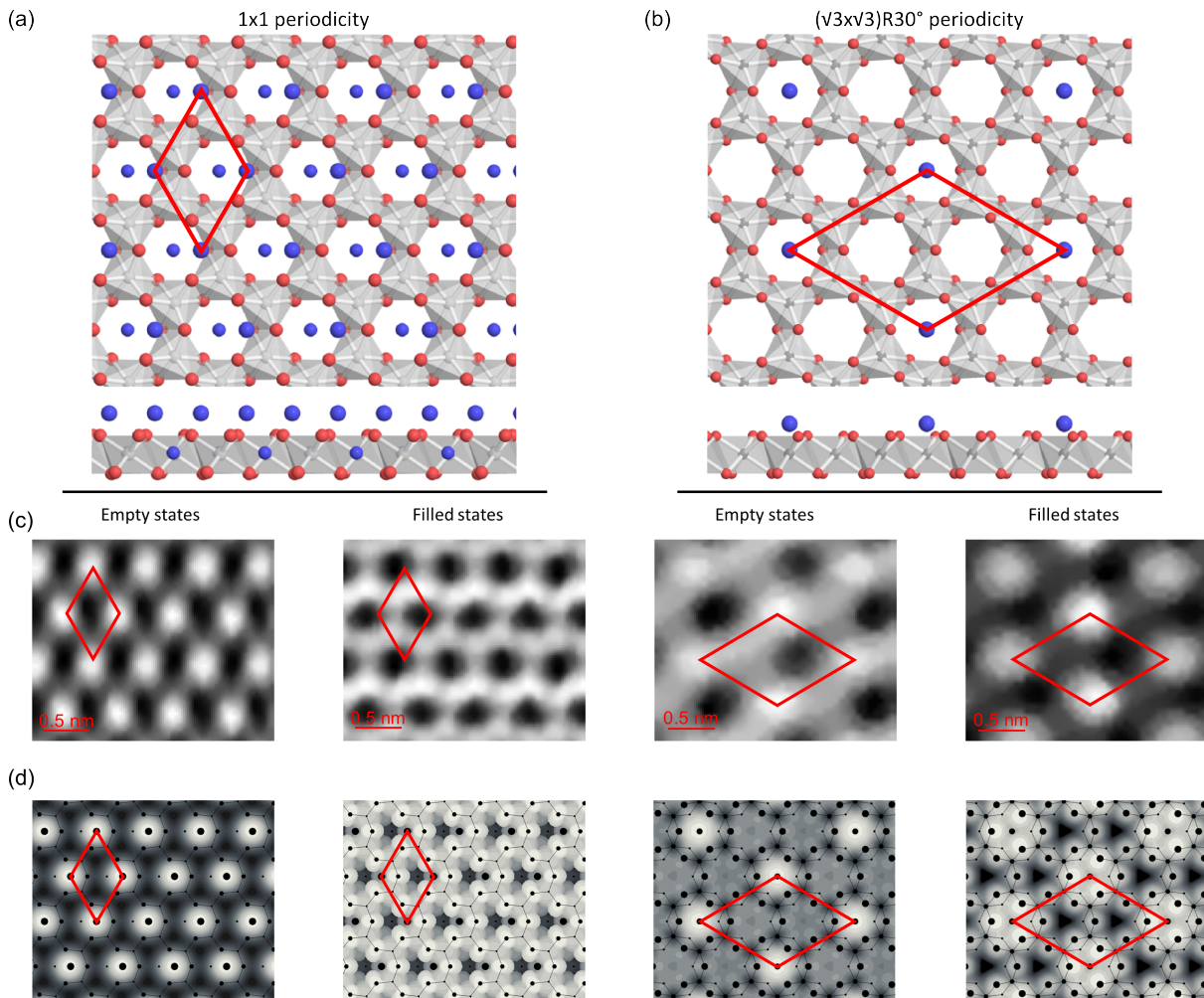


FIG. 2. (Color online) (a,b) Theoretically determined structural models for 1×1 and $(\sqrt{3} \times \sqrt{3})R30^\circ$ surfaces viewed from the top and side, respectively (Na: blue, Ir: gray, O: red). Na atoms in the topmost layer are shown larger for clarity. (c) Experimental and (d) theoretically simulated STM images at $V_{\text{bias}} = \pm 2$ V. On the 1×1 surface, there is a clear contrast reversal between empty and filled states. On the $(\sqrt{3} \times \sqrt{3})R30^\circ$ surface, the dominant bright features for empty and filled images are located at the same positions.

base pressure of $p < 10^{-10}$ mbar. After immediate transfer to a home-built low temperature scanning tunneling microscope (STM) operating at 80 K, the surface was investigated by STM and STS. The latter allows mapping of occupied and unoccupied states as well as simultaneous access to spatial variations in the electronic surface properties [9, 10]. On the freshly cleaved surface, two different stable surface terminations were found in constant-current topographic (CCT) measurements both showing atomic level resolution (Fig. 1). The periodicity of the terminated surfaces suggests cleaving along the ab -plane of the crystal. One termination shows the periodicity of bulk Na₂IrO₃ and is labeled as 1×1 in the following. The second termination shows a $(\sqrt{3} \times \sqrt{3})R30^\circ$ reconstruction with respect to the 1×1 . The two terminations occur in roughly the same proportion. While the 1×1 surface shows a long-range periodic structure over tens

of nanometers, the $(\sqrt{3} \times \sqrt{3})R30^\circ$ surface exhibits lots of defects and is well-ordered only on the scale of a few nanometers.

The cleavage process almost certainly leaves the strongly bonded IrO₆ octahedra intact. Hence, the observation of two different surface terminations suggests that cleaving creates two metastable surfaces with different Na coverage and hence different periodicity. We used DFT to determine the equilibrium geometries of different candidate surfaces with varying Na content in the top layer as well as subsurface layers. Total energies and forces were calculated within the PBE generalized-gradient approximation using projector-augmented-wave potentials, as implemented in VASP [11, 12]. After relaxation, we simulated STM images using the method of Tersoff and Hamann [13], by integrating the local density of states (LDOS) within ± 2 eV around the Fermi level. The sur-

face of constant integrated LDOS then corresponds to the ideal STM topography at that bias voltage.

Figure 2 shows the theoretical equilibrium structure and STM imagery for the two models that best reproduce the imagery of the two observed surfaces. The 1×1 surface shown in Fig. 2(a) was constructed by starting from the bulk crystal, which consists of stacked atomic layers in the stoichiometric sequence $\dots | \text{Na}_3 | \text{O}_3 | \text{Na}_1, \text{Ir}_2 | \text{O}_3 | \dots$. By cleaving this crystal within the pure Na layer one obtains surfaces with different relative Na content. For reference, the ideal stoichiometric surface has a $\text{Na}_{3/2}$ surface layer. We constructed the 1×1 surface in Fig. 2(a) by removing one-third of the Na atoms from this idealized surface. Hence the model in Fig. 2(a) is $\text{Na}_1 | \text{O}_3 | \text{Na}_1, \text{Ir}_2 | \text{O}_3 | \dots$. The agreement between simulated and measured constant-current topographies is excellent, strongly suggesting that this structural model is correct. In particular, the strong contrast inversion between empty and filled states observed experimentally is well reproduced in the simulated images. Even the detailed topography agrees well: The filled states appear as a bright honeycomb network, while the empty states appear as disconnected bright spots. The contrast reversal arises from different tunneling paths for positive and negative biases, via empty Na states and filled O states, respectively.

Figure 2(b) shows an even more substoichiometric surface created by removing the entire topmost Na layer as well as two-thirds of the Na atoms in the subsurface Ir-Na layer. The nominal structure of this surface is hence $\text{O}_3 | \text{Na}_{1/3}, \text{Ir}_2 | \text{O}_3 | \dots$, which indeed has the experimentally observed $(\sqrt{3} \times \sqrt{3})R30^\circ$ periodicity [14]. Upon relaxation the Na atoms in the subsurface layer move upwards by nearly 2 Å from their ideal positions. Hence the equilibrium surface structure is actually $\text{Na}_{1/3} | \text{O}_3 | \text{Ir}_2 | \text{O}_3 | \dots$, as shown in Fig. 2(b). This very large relaxation is confirmed experimentally by the excellent agreement between experimental and simulated empty-state images: Both the periodicity and topography are entirely determined by empty Na states, which only be the case if the Na atoms have relaxed completely out of the subsurface Ir layer. The filled-state images are also in very good agreement. Interestingly, they do not show any contrast reversal. Instead, the topography in filled-state images actually arises from oxygen orbitals that are neighbors of surface Na atoms, whereas the empty-state images are dominated by the unoccupied Na orbitals themselves.

We next performed a spectral analysis using scanning tunneling spectroscopy (STS) of the two surface terminations to investigate their electronic structure. Figure 3(a) shows the differential conductivity, dI/dV , of both surface structures. The current noise level of 700 fA allows us to estimate the band gaps to be $E_g \approx 1$ eV on the 1×1 surface and $E_g \approx 0.5$ eV on the $(\sqrt{3} \times \sqrt{3})R30^\circ$ surface. One might be tempted to compare these num-

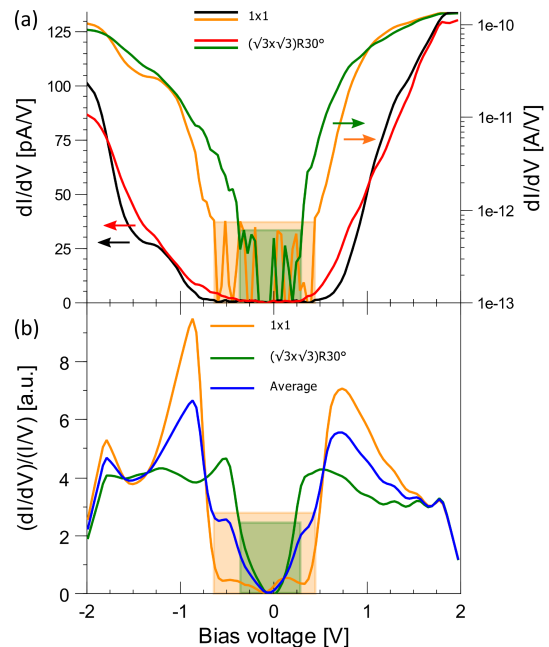


FIG. 3. (Color online) (a) Differential conductivity spectra of the 1×1 and $(\sqrt{3} \times \sqrt{3})R30^\circ$ surface plotted on linear and logarithmic scales (left and right, respectively). The region of zero tunnel current within the current detection limit of the present setup (700 fA) is identified as the band gap and is indicated in (a) and (b) as shaded areas with colors corresponding to the graphs. The 1×1 surface band gap can be estimated to $E_g \approx 1$ eV, while the $(\sqrt{3} \times \sqrt{3})R30^\circ$ surface shows a smaller band gap of $E_g \approx 0.5$ eV. (b) Normalized differential conductivity graphs of the two surfaces and their average. Spectral features are visible at $V_{\text{bias}} \simeq \pm 1$ V. The averaged spectrum, corresponding to equal surface coverages, allows a comparison to ARPES and optical conductivity measurements. The data within the shaded areas is below the resolution limit of our setup and apparent features are only the result of the calculation process [15].

bers, especially the less strongly reconstructed 1×1 , with the optical and ARPES band gap of 340 meV reported in Ref. 16. However, this discrepancy must be taken with a grain of salt because optical absorption is a bulk probe and it is only natural that the surface gap, after reconstruction and relaxation, is very different—including the effects of the less well-screened Hubbard U at the surface.

Regarding ARPES, which is indeed a surface probe, in order to access the excitation gap, in Ref. 16 the surface of Na_2IrO_3 was coated with K, to shift the chemical potential into the upper Hubbard band. As we observe a 500 meV difference between different Na_2IrO_3 surfaces, there is no question that coating with K should have a serious effect on the gap. Moreover, it is also expected that the surface in [16] probably also consisted of an ensemble of two reconstructions as found here. Hence to directly compare the surface gap obtained from STS and K-doped ARPES, all these issues need to be considered.

Comin *et al.* pointed out that the one-electron hop-

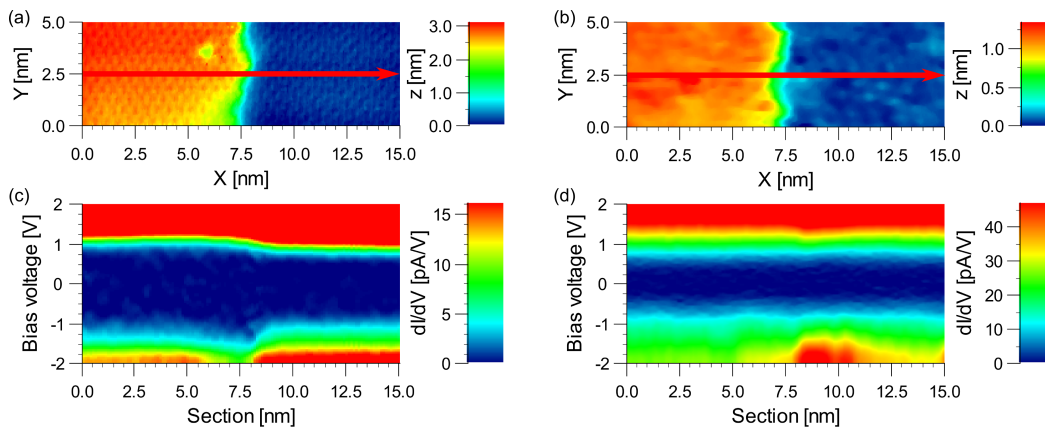


FIG. 4. (Color online) (a) STM topography of a surface step between two equivalent 1×1 surfaces. The step height is $h \approx 26.5$ Å, corresponding to five unit cells of Na_2IrO_3 . (b) Topography of a surface step separating two equivalent $(\sqrt{3} \times \sqrt{3})\text{R}30^\circ$ surfaces. The step height is $h \approx 10.6$ Å, corresponding to two unit cells. (c) Differential conductivity spectra along the red line in (a). We observe a smooth transition and a slightly larger gap on the upper terrace. The full band gap is evident throughout the line scan. (d) Differential conductivity spectra along the red line in (b). The band gap is maintained across the step edge with only small fluctuations within the valence and conduction bands.

ping, combined with spin-orbit coupling, alters the band structure substantially compared with the spin-orbit-only picture of two $J_{\text{eff}} = 1/2$ and $3/2$ level. In particular, it creates a pseudogap in the center of the $J_{\text{eff}} = 1/2$ band, which is then enhanced into a full gap by Hubbard correlations [16]. Similarly, the $J_{\text{eff}} = 3/2$ quartet is, because of hybridization with $J_{\text{eff}} = 1/2$, split into three separated manifolds. The calculated DOS [see Ref. 16, Fig. 4(e-f)] clearly demonstrates this feature. Angle-integrated photoemission spectra [16] between -2 eV and 0 eV were decomposed into four Gaussians, corresponding to the four bands described above, at the positions $-0.5, -1, -1.4$, and -1.9 eV, with weights roughly corresponding (given the possible energy dependence of the matrix elements) to 1:2:1:1, consistent with the band structure calculation [7].

Our experimental DOS, which we estimate in Fig. 3(b) by averaging the normalized conductivity, $(dI/dV)/(I/V)$, over the two surfaces, is largely consistent with this observation. We note that the higher-bias DOS is somewhat overestimated in the measurements, probably due to incomplete cancellation of the tunneling matrix elements and the band edges are distorted due to the calculation process. It is worth noting that in Ref. 16, as well as in our experiment, the centers of the occupied bands are shifted by 0.1 to 0.3 eV to lower energies which would also increase the minimal gap.

Nevertheless, the decomposition of the angle integrated photoemission spectra between -2 eV and 0 eV corresponding to the four bands described above and the consistence with theory might be fortuitous. Indeed, accurate modeling of the ARPES spectra may require including spectral features of both surface reconstructions (with similar weights), as suggested by our structural

analysis.

Comparing our results with Ref. 16, the significantly larger band gap found in STS remains an open issue. As ARPES does not directly provide the band gap value, the evolution of ARPES spectra on coating the surface with K was used to determine this value. While Ref. 16 discussed the deposition of K only as doping, another reasonable process is the transformation of the $(\sqrt{3} \times \sqrt{3})\text{R}30^\circ$ surface as K is incorporated. Such a global change of the ratio of 1×1 and $(\sqrt{3} \times \sqrt{3})\text{R}30^\circ$ reconstructed areas may also result in a modified ARPES spectrum with a shift of spectral weight to higher binding energies.

Considering the STS spectra, tip-induced band bending might be a possible candidate to explain an apparent increase of the band gap. Our topographic data shows that the surfaces exhibits atomic scale defects leading to the expectation of Fermi level pinning inside the band gap similar to results on semiconductor surfaces [17]. This scenario implies that STS does indeed reflect a significantly larger surface band gap.

Finally, we address the issue of QSH behavior. Ref. 2 predicted that Na_2IrO_3 is a QSH insulator and therefore that the band gap must briefly close as a step is traversed. However, as we have established, the surface of Na_2IrO_3 is rather different from the bulk. Even if the model of Ref. 2 correctly captures the relevant features of the bulk band structure, it may be not applicable to the actual surfaces that are realized in nature. With this caveat in mind, we have monitored the tunneling gap as the tip traverses a step (Fig. 4). The observed step heights are in agreement with the crystal structure [18] and correspond to the height of five unit cells (26.5 Å) and two unit cells (10.6 Å), respectively. Figures 4(c) and (d) show spatially

resolved STS spectra taken along the red lines in Figs. 4(a) and (b). Upon traversing a step separating two 1×1 surfaces, a smooth transition can be observed with no sign of gap closure anywhere. The step separating two $(\sqrt{3} \times \sqrt{3})R30^\circ$ regions likewise shows a constant band gap with no sign of closure. We conclude that neither of the two possible terminations of Na_2IrO_3 shows any evidence of the QSH effect.

Work supported by the German Science Foundation through SPP 1666 and the Helmholtz Virtual Institute 521. This work was also supported in part by the U.S. Office of Naval Research through the Naval Research Laboratory's Basic Research Program.

* Corresponding author.
mwender@gwdg.de

- [1] B.J. Kim, H. Ohsumi, T. Komesu, S. Sakai, T. Morita, H. Takagi, T. Arima, *Science* **323** 1329 (2009).
- [2] A. Shitade, H. Katsura, J. Kunes, X.-L. Qi, S.-C. Zhang, N. Nagaosa, *Phys. Rev. Lett.* **102**, 256403 (2009).
- [3] D. Pesin and L. Balents, *Nature Phys.* **6** 376 (2010).
- [4] J. Chaloupka, G. Jackeli, and G. Khaliullin *Phys. Rev. Lett.* **105**, 027204 (2010).
- [5] Hong-Chen Jiang, Zheng-Cheng Gu, Xiao-Liang Qi, S. Trebst, *Phys. Rev. B* **83** 245104 (2011).
- [6] I. I. Mazin, H. O. Jeschke, K. Foyevtsova, R. Valentí, D. I. Khomskii, *Phys. Rev. Lett.* **109**, 197201 (2012).
- [7] K. Foyevtsova, H. O. Jeschke, I. I. Mazin, D. I. Khomskii, R. Valentí, *Phys. Rev. B* **88**, 035107 (2013).
- [8] Y. Singh and P. Gegenwart, *Phys. Rev. B* **82**, 064412 (2010).
- [9] R. M. Feenstra, P. Mårtensson, *Phys. Rev. Lett.* **61**, 447-450 (1988)
- [10] C. Ye, P. Cai, R. Yu, X. Zhou, W. Ruan, Q. Liu, C. Jin, Y. Wang, *Nat. Commun.* **4**, 1365 (2013)
- [11] G. Kresse and J. Hafner, *Phys. Rev. B* **47**, 558 (1993).
- [12] G. Kresse and J. Furthmüller, *Phys. Rev. B* **54**, 11169 (1996).
- [13] J. Tersoff, D. R. Hamann, *Phys. Rev. B* **31**, 805 (1985)
- [14] Although it is possible to construct surface models having $(\sqrt{3} \times \sqrt{3})R30^\circ$ periodicity without fully depleting the topmost Na layer, these are strongly contradicted by the observed STM topography.
- [15] J. A. Stroscio, R. M. Feenstra and A. P. Fein, *Phys. Rev. Lett.* **57**, 2579-2582 (1986)
- [16] R. Comin, G. Levy, B. Ludbrook, Z.-H. Zhu, C.N. Venstra, J.A. Rosen, Y. Singh, P. Gegenwart, D. Stricker, J.N. Hancock, D. van der Marel, I.S. Elfimov, A. Damascelli, *Phys. Rev. Lett.* **109**, 266406 (2012).
- [17] R. M. Feenstra, Y. Dong, M. P. Semtsiv and W. T. Maselink, *Nanotechnology* **18**, 044015 (2007)
- [18] S. K. Choi, R. Coldea, A. N. Kolmogorov, T. Lancaster, I. I. Mazin, S. J. Blundell, P. G. Radaelli, Y. Singh, P. Gegenwart, K. R. Choi, S.-W. Cheong, P. J. Baker, C. Stock, and J. Taylor, *Phys. Rev. Lett.* **108**, 127204 (2012).